Robust On-line Obstacle Detection using Range Data for Reactive Navigation ⋆

José Miguel Vilca **Lounis Adouane** **Youcef Mezouar**

Institut Pascal, UBP – UMR CNRS 6602, Clermont-Ferrand, France
(e-mail: Jose_Miguel.Vilca_Ventura@univ-bpclermont.fr)

Abstract: This paper proposes a robust on-line and adaptive elliptic trajectory for reactive obstacle avoidance. These trajectories permit a safe and smooth mobile robot navigation in cluttered environment. Indeed, they use limit-cycle principle already applied in the literature Adouane et al. (2011). The main contribution proposed here is to perform this navigation in a completely reactive way while using only uncertain range data. Each obstacle, in this obstacle avoidance strategy, is surrounded by an ellipse and its parameters are obtained online while using the sequence of uncertain range data. This method uses the fusion between heuristic approach and Extended Kalman Filter (EKF) techniques to improve the computed ellipse parameters. A large number of simulations and experiments show the efficiency of the proposed on-line navigation in cluttered environment.

Keywords: Mobile robots navigation; Obstacle detection and avoidance; Telemetry; Parameter identification; Extend Kalman Filter.

1. INTRODUCTION

An important issue for successful mobile robot navigation is obstacle avoidance. This function permits to prevent robot collision and insure thus robot safety. One area of research in obstacle avoidance is concentrated on reactive methods, where only local sensors information is used rather than a prior knowledge of the environment Toibero et al. (2007), Adouane (2009a). In Khatib (1986), the author proposes a real-time obstacle avoidance approach based on the principle of artificial potential fields. In this work, it is assumed that the robot actions are guided by the sum of attractive and repulsive fields.

Many other approaches can be found in the literature, such as the obstacle avoidance algorithm based on orbital trajectories. It is described by circular limit-cycle differential equations Kim and Kim (2003), Jie et al. (2006) or Adouane (2009b). This work uses elliptical trajectories that was presented in Adouane et al. (2011). Therefore, more generic and efficient obstacle avoidance is performed and this even with different obstacle shapes, for instance long walls. In fact, an ellipse fit better this kind of obstacles than a circle.

At this aim, different approaches have been proposed in the literature to enclose the data with an ellipse Welzl (1991) and Zhang (1997). In Welzl (1991), the author proposed a technique to obtain the smallest enclosing ellipse by a set of data using primitive operation with linear increasing time with regards to data dimension. In Zhang (1997), the author presents a summary of the methods to fit a set of data with an ellipse. The presented methods are the least square fitting based on algebraic and Euclidean distance, Kalman filtering method and robust estimation.

The Extended Kalman Filter has important application in different fields, such as parameters estimation, data fusion and signal processing Xiong et al. (2011) and Fouque et al. (2008). In robotics field, the main applications is found in localization, data fusion of the sensor and mapping Rigatos (2010) and Levinson and Thrun (2010). In this work, we use the EKF to enhance the ellipse parameters obtained from uncertain data.

The rest of the paper is organized as follows: in the next section, the task of navigation using elliptic trajectories is presented. In section 3, the details of the control architecture are introduced and obstacle avoidance algorithm is given. Section 4 presents the method for enclosing the uncertain range data with an ellipse. Simulation and experimental results are given in section 5. Finally, conclusion and some future works are given in section 6.

2. NAVIGATION IN CLUTTERED ENVIRONMENT

First, let us assume that the obstacle O can be surrounded by an elliptical box (cf. Fig. 1). The elliptical shape is represented by its Cartesian form:

$$\frac{(x-h)^2}{a^2} + \frac{(y-k)^2}{b^2} = 1 \qquad (1)$$

where $(h, k) \in \Re^2$ are the ellipse center coordinates and $a, b \in \Re^+$ are the semi-axes with $a \geq b$.

The choice of ellipse box rather than circle as used in Adouane et al. (2011) is to have one more generic and flexible mean to surround and fit accurately different kind of obstacles shapes (longitudinal shapes). In section 4, it will be shown how the ellipse parameters can be efficiently

⋆ Supported by the French National Research Agency (ANR) through the Safeplatoon and R-Discover projects.

computed from range data. Let us also represent the robot and the target by circles C_R and C_T of radius R_R and R_T respectively (cf. Fig. 1). One can define:

(1) D_{RO} as the minimal distance between the robot and the obstacle "O".
(2) *Ellipse of influence* (E_f) as an ellipse that has the same center (h, k) and tilt angle Ω as the ellipse which surround the obstacle (1) while its major and minor semi-axes, a_{lc} and b_{lc}, are defined as follows

$$\begin{cases} a_{lc} = a + R_R + Margin \\ b_{lc} = b + R_R + Margin \end{cases}$$

where *Margin* represents safety tolerances encapsuling: perception uncertainties, control reliability and accuracy.
(3) "l" as the line passing through the center of C_R and C_T. As we will see in the sequel, our method only needs to know if it exists intersection points between l and E_f (cf. Fig. 1).

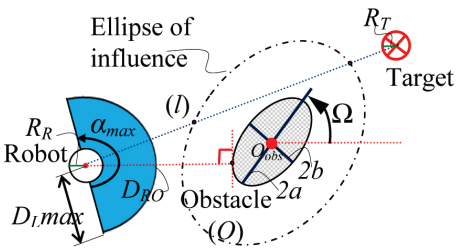

Fig. 1. The obstacle and robot modeling.

The objective of the navigation task in cluttered environment is to lead a mobile robot towards a specific target in an unstructured environment. This task must be achieved while avoiding static and dynamic obstacles O which can have different shapes.

3. CONTROL ARCHITECTURE

The used control structure is based on Benzerrouk et al. (2010) (cf. Fig. 2). It aims to manage the interactions between elementary controllers while guaranteeing the stability of the overall control as proposed in Adouane (2009a). Its objective is also to insure safe, smooth and fast robot navigation. The specific blocks composing the global control are detailed below.

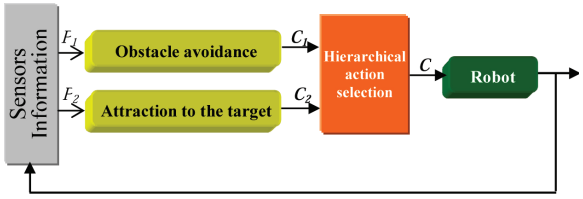

Fig. 2. Control architecture for mobile robot navigation.

This control architecture uses a hierarchical action selection mechanism to manage the switches between the controllers, according to environment perception. The mechanism activates the obstacle avoidance controller as soon as it exists at least one obstacle which can obstruct the future robot movement toward its target Adouane (2009b). This allows to anticipate the activation of obstacle avoidance controller unlike what is proposed in Brooks (1986) or Adouane and Le Fort-Piat (2006), which wait until the robot is in the immediate vicinity of the obstacle (i.e. $D_{RO} \leq R$ "a certain radius value").

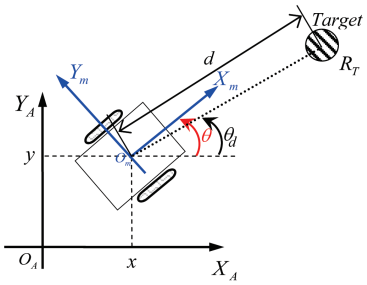

Fig. 3. Robot configuration in a Cartesian reference frame.

Before describing each elementary controller, let us briefly recall the kinematic model of an unicycle robot (cf. Fig. 3)

$$\begin{bmatrix} \dot{x} \\ \dot{y} \\ \dot{\theta} \end{bmatrix} = \begin{bmatrix} cos(\theta) & 0 \\ sin(\theta) & 0 \\ 0 & 1 \end{bmatrix} \begin{bmatrix} v \\ \omega \end{bmatrix} \quad (2)$$

where x, y, θ are configuration state of the unicycle at the point O_m, v and ω are respectively, the linear and the angular velocity of the robot at the point O_m.

3.1 Attraction to target controller

This controller guides the robot toward the target which is represented by a circle C_T of center (x_T, y_T) and radius R_T (cf. Fig. 3). This controller is based on the position control of the robot to the target, represents by d and θ_d in Fig. 3, more details are given in Benzerrouk et al. (2010). As we consider a circular target with radius R_T, therefore, to guarantee that the center of robot axes reaches the target with asymptotical convergence, d must be $\leq R_T$. (cf. Fig. 3). The position errors are:

$$\begin{cases} e_x = x - x_T = d\cos(\theta_d) \\ e_y = y - y_T = d\sin(\theta_d) \end{cases} \quad (3)$$

where d is the distance of the robot to the target and θ_d is the orientation of the line passing through the robot and the target. $\tilde{\theta} \in [-\pi, \pi]$ is the orientation error, such that

$$\tilde{\theta} = \theta_d - \theta \quad (4)$$

Its derivative $\dot{\tilde{\theta}}$ is then

$$\dot{\tilde{\theta}} = \dot{\theta}_d - \omega \quad (5)$$

From the previous equation and the kinematic model (2), we obtain

$$\dot{\theta}_d = \omega_r = v\sin(\tilde{\theta})/d \quad (6)$$

where v is the linear velocity of the robot and $d > 0$.

3.2 Obstacle avoidance controller

To perform the obstacle avoidance behavior, the robot needs to follow accurately limit-cycle trajectories as detailed in Kim and Kim (2003) or Adouane (2009b). In these

works, the authors use a circular limit-cycle characterized by a circle of influence of radius R_I. In Adouane et al. (2011), it is proposed to extend this methodology for more flexible limit-cycle shape (an ellipse). The main ideas of this controller are detailed below.

The differential equations giving elliptic limit-cycles are:

$$\dot{x}_s = \ my_s + x_s(1 - x_s^2/{a_{lc}}^2 - y_s^2/{b_{lc}}^2 - cx_s y_s) \quad (7)$$

$$\dot{y}_s = -mx_s + y_s(1 - x_s^2/{a_{lc}}^2 - y_s^2/{b_{lc}}^2 - cx_s y_s) \quad (8)$$

with $m = \pm 1$ according to the direction of avoidance (clockwise or counter-clockwise, cf. Fig. 4). (x_s, y_s) corresponds to the position of the robot according to the center of the ellipse; a_{lc} and b_{lc} characterize respectively the major and minor elliptic semi-axes (cf. Fig. 1); c if $\neq 0$ gives the Ω ellipse angle.

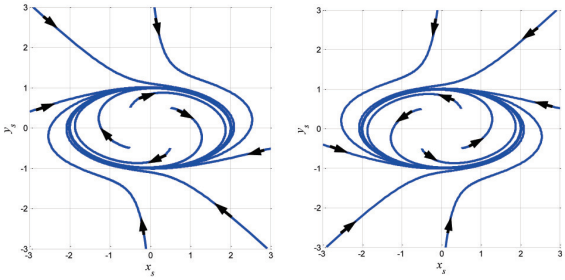

Fig. 4. Clockwise and counter-clockwise shape for the used elliptic limit-cycles.

The algorithm for obstacle avoidance is summarized by following main steps:

- The nearest hindering obstacle is detected,
- The direction of avoidance is chosen according to the position of the robot with regards to the position of the obstacle and the target,
- The robot avoids the obstacle while following an elliptic limit cycle trajectory which has the semi-axes a_{lc} and b_{lc}, with $a_{lc} \geq b_{lc}$.

Refer to Adouane et al. (2011) for details. The desired robot orientation is thus given by the differential equation of the limit-cycle (7) and (8) as:

$$\theta_d = arctg\,(\dot{y}_s/\dot{x}_s) \quad (9)$$

and the error by:

$$\tilde{\theta} = \theta_d - \theta \quad (10)$$

3.3 Control law

The used control law is expressed as follows Benzerrouk et al. (2010):

$$v = v_{max} e^{-1/d} cos(\tilde{\theta}) \quad (11)$$

$$\omega = \quad \omega_r + K_p \tilde{\theta} \quad (12)$$

where v_{max} is the maximum linear velocity, K_p is a constant such that $K_p > 0$ and d is the distance between the robot and the target when the *attraction to the target* controller is activated, and d is equal to D_{RO} if the *obstacle avoidance* is activated (cf. Fig. 1). The robot reaches the target when $0 < d \leq R_T$.

It is interesting to notice that only one control law is applied to the robot even if the control architecture contains two different controllers. Only the set points change according to the applied controller, Benzerrouk et al. (2010).

4. ENCLOSING UNCERTAIN RANGE DATA WITH AN ELLIPSE

During the robot movement, it is important to detect online and to avoid the hinder obstacle. At this aim, the observed noisy range data are surrounded with the closest ellipse to apply elliptic limit-cycle approach.

For this purpose, let us consider a set of n points in $\Re^2$ with coordinates $P_i(x_i, y_i)$ (cf. Fig. 5). These points are computed from the data range of the robot, and the outliers are erased while using the Mahalanobis distance De Maesschalck et al. (2000). In this section, it will be shown how to compute the ellipse that encloses all points. An important condition in this work is that the methods need to start at least with three different points.

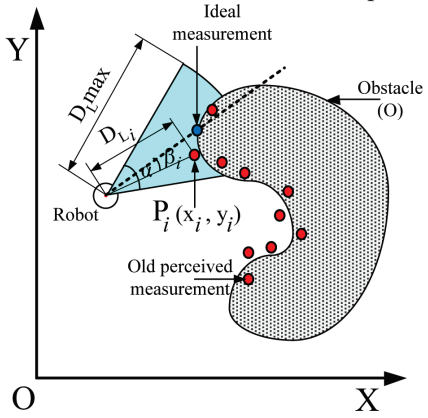

Fig. 5. Range sensor model and data set of n points.

Before describing below the proposed methods to obtain the enclosing ellipse, let us present the model of the perceived data from range sensor in the following subsection.

4.1 Range sensor model

The position of the obstacle with respect to the range sensor in $\Re^2$ can be denoted by the polar coordinates (D_{Li}, β_i), where D_{Li} is the distance between the center of the robot and the impact point of the sensor and β_i is the orientation with respect to the mobile reference frame (cf. Fig 5).

The sensor specifications and the real behavior of the sensor has significant differences Burguera et al. (2009). In this work, we focus on the accuracy of the range sensor, because we have observed that short range readings are more accurate than the long range ones. In Burguera et al. (2009) it is observed how the mean and the standard deviation of the errors between the real and the measured range tend to increase with distance.

The reading range data provided by the range sensor at each time step is modeled by the Normal distribution $D_{Li}^t = N(\hat{D}_{Li}^t,\ P_{Li}^t)$, where $\hat{D}_{Li}^t$ is the mean vector and P_{Li}^t is the covariance that is defined as the model of the range and angular uncertainties. The angular uncertainty is related to the sonar opening α and the range uncertainty is given according to the accuracy of the range sensor (cf. Fig. 5) Burguera et al. (2009).

The following sub-sections will present the proposed methods to enclose the data with an ellipse. Sub-section 4.2

permits to address the problem of enclosing ellipse and the sub-section 4.3 is the extension of the proposed method to deal with uncertainty data and to enhance the identification of the ellipse parameters to get round the obstacle.

4.2 Heuristic approach

The proposed heuristic approach uses the distance between the points to obtain one of the axes.

This method computes the distance between all the points $d_{ij} = \|p_i - p_j\|$ with $i, j = 1, \ldots, n$; and select the maximum distance d_{max}. We have thus, $d_{ij} \leq d_{max}$. This d_{max} is not decreasing if more data points are added. While connecting the points with the maximum distance, one of the ellipses axes is obtained. The ellipse center C_O is the middle point between the points with maximum distances and the first semi-axis is $a_1 = d_{max}/2$ (cf. Fig 6).

Now, we work in the new coordinates system $X'Y'$ to obtain the second ellipse semi-axis a_2. We transform the n points to new coordinates system using (13).

$$\mathbf{P}'_i = \begin{bmatrix} cos(\Omega) & sin(\Omega) \\ -sin(\Omega) & cos(\Omega) \end{bmatrix} (\mathbf{P}_i - \mathbf{C}_O) \tag{13}$$

Where Ω is the orientation of the line between the two points that have the maximum distance. $\mathbf{P}'_i(x'_i, y'_i)$ is the coordinate in the new system, $\mathbf{P}_i(x_i, y_i)$ is the coordinate in the initial system and $\mathbf{C}_O$ is the coordinate of the ellipse center in the initial system.

If the value of $|y'_i|$ of the points is greater than a threshold $\epsilon > 0$, the distance of $\mathbf{P}'_i$ to the origin O' is computed, i.e., if $|y'_i| > \epsilon \Rightarrow d'_i = \|\mathbf{P}'_i\|$ is computed. This threshold is used to eliminate the points that are colinear with the two points that have the maximum distance (first axis) and the points in the perpendicular line to first axis (which could produce a large axis).

We know that all points inside the ellipse have the distance $d'_i < max\{a_1, a_2\}$. As we do not know the spatial distribution of the set of points and to ensure that all the points are inside the ellipse, we choose that $a_2 = max\{b_i\}$, where b_i is the computed semi-axis using $\mathbf{P}'_i$ in (1). In other words, $b_i \leq a_2 \leq max\{a_1, a_2\} \Rightarrow \mathbf{P}_i \in Ellipse$. Hence, the ellipse encloses all points without regard of the obstacle shape. Finally, we obtain the semi-axes of the ellipse (1), cf. Fig 6, such as:

$$\begin{aligned} a &= max\{a_1, a_2\} \\ b &= min\{a_1, a_2\} \end{aligned} \tag{14}$$

The orientation of the ellipse is $\Omega_E = \Omega + \Pi/2$ if a_2 is the major axis, otherwise $\Omega_E = \Omega$. The heuristic approach is an efficient method to enclose data with an ellipse, however, this method does not consider neither uncertain data nor the sequentiality of obtained data which characterize the real experiments. The following subsection deal with this issue.

4.3 Optimal parameters identification using EKF

Kalman filter is likely to have applications in many fields as a general method for integrating noisy measurements Rigatos (2010) and Levinson and Thrun (2010).

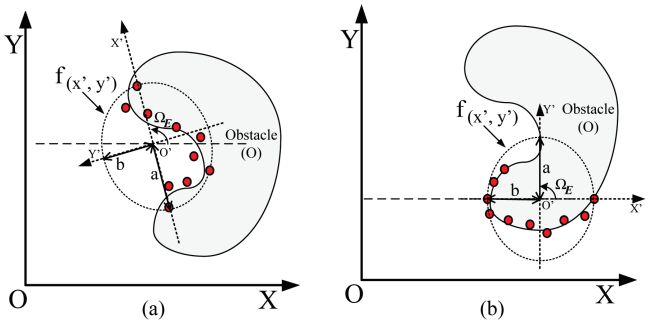

Fig. 6. Obtained ellipse using heuristic approach for two data set of points.

This approach uses the general conic equation which is given by:

$$f(x, y) = Ax^2 + 2Bxy + Cy^2 + 2Dx + 2Ey + F = 0 \tag{15}$$

According to the real constants A, B, C, D, E anf F, we obtain the analytic equation of the different kind of conics (parabola, ellipse and hyperbole). An ellipse is defined if the conic parameters (15) satisfy the following condition $B^2 - AC < 0$.

The problem is to fit a conic section (15) with a set of n points $\{p_i\} = \{(x_i, y_i)\} \,|\, i = 1, \ldots, n$. This set of points are selected using (15) with the ellipse parameters from the heuristic method. These points satisfy the following condition $|f(x_i, y_i)| < \delta$, and $0 < \delta << 1$, i.e., these points are close to the boundary of the obtained ellipse, other points are not consider for this method. As the data are noisy, it is unlikely to find a set of parameters (A, B, C, D, E, F) (except for the trivial solution $A = B = C = D = E = F = 0$) such that $f(x_i, y_i) = 0$.

We applied this method to the conic fitting. The state vector is defined by the conic parameters as $\mathbf{x} = [A, B, C, D, E, F]^T$ and the measurement vector by the point as $\mathbf{z}_i = [x_i, y_i]^T$, a linear dynamic system (in discrete-time form) can be described by

$$\mathbf{x}_{i+1} = \mathbf{F}_i \mathbf{x}_i + \mathbf{w}_i \tag{16}$$

$$\mathbf{z}_i = \mathbf{H}_i \mathbf{x}_i + \mathbf{v}_i \tag{17}$$

where $i = 0, 1, \ldots$. The matrix state $\mathbf{F}_i$ is the identity matrix of order 6 ($\boldsymbol{I}_6$), $\mathbf{w}_i$ is the vector of random disturbance of the state and is usually modeled as white noise:

$$E[\mathbf{w}_i] = 0, \qquad E[\mathbf{w}_i \mathbf{w}_i^T] = \mathbf{Q}_i$$

The measurement equation (17) is nonlinear and it is described by the observation function:

$$f_i(\mathbf{z}'_i, \mathbf{x}_i) = x_i'^2 A + 2x'_i y'_i B + y_i'^2 C + 2x'_i D + 2y'_i E + F \tag{18}$$

where $\mathbf{z}'_i$ is the ideal measurement. The real measurement $\mathbf{z}_i$ is assumed to be corrupted by additive noise $\mathbf{v}_i$, i.e. $\mathbf{z}_i = \mathbf{z}'_i + \mathbf{v}_i$. We expand $f_i(\mathbf{z}'_i, \mathbf{x}_i)$ into a Taylor series about $(\mathbf{z}_i, \hat{\mathbf{x}}_{i|i-1})$:

$$\begin{aligned} f_i(\mathbf{z}'_i, \mathbf{x}_i) = \quad & f_i(\mathbf{z}_i, \hat{\mathbf{x}}_{i|i-1}) + \frac{\partial f_i(\mathbf{z}_i, \hat{\mathbf{x}}_{i|i-1})}{\partial \mathbf{z}'_i}(\mathbf{z}'_i - \mathbf{z}_i) \\ & + \frac{\partial f_i(\mathbf{z}_i, \hat{\mathbf{x}}_{i|i-1})}{\partial \mathbf{x}_i}(\mathbf{x}_i - \hat{\mathbf{x}}_{i|i-1}) + O((\mathbf{z}'_i - \mathbf{z}_i)^2) \\ & + \qquad O((\mathbf{x}_i - \hat{\mathbf{x}}_{i|i-1})^2) \end{aligned} \tag{19}$$

By ignoring the second order terms, we get a linearized measurement equation:

$$\mathbf{y}_i = \mathbf{M}_i \mathbf{x}_i + \xi_i \tag{20}$$

where $\mathbf{y}_i$ is the new measurement vector, ξ_i is the noise vector of the new measurement, and $\mathbf{M}_i$ is the linearized transformation matrix. They are given by

$$\mathbf{M}_i = \frac{\partial f_i(\mathbf{z}_i, \hat{\mathbf{x}}_{i|i-1})}{\partial \mathbf{x}_i}$$

$$\mathbf{y}_i = -f_i(\mathbf{z}_i, \hat{\mathbf{x}}_{i|i-1}) + \frac{\partial f_i(\mathbf{z}_i, \hat{\mathbf{x}}_{i|i-1})}{\partial \mathbf{x}_i} \hat{\mathbf{x}}_{i|i-1}$$

$$\xi_i = \frac{\partial f_i(\mathbf{z}_i, \hat{\mathbf{x}}_{i|i-1})}{\partial \mathbf{z}'_i} (\mathbf{z}'_i - \mathbf{z}_i)$$

Clearly, we have $E[\xi_i] = 0$, and $E[\xi_i \xi_i^T] = R_{\xi_i}$. We consider then there is no correlation between the noise process of the system and that of the observation. The derivative of $f_i(\mathbf{z}_i, \mathbf{x})$ with respect to $\mathbf{x}$ and that with respect to $\mathbf{z}_i$, are given by

$$\frac{\partial f_i(\mathbf{z}_i, \mathbf{x})}{\partial \mathbf{x}} = [x_i^2,\ 2x_i y_i,\ y_i^2,\ 2x_i,\ 2y_i,\ 1] \tag{21}$$

$$\frac{\partial f_i(\mathbf{z}_i, \mathbf{x})}{\partial \mathbf{z}_i} = 2[x_i A + y_i B + D,\ y_i C + x_i B + E] \tag{22}$$

The extended Kalman Filter (EKF) is then described by the well known following steps:

- Initialization: $\Pi_{0|0} = \Pi_0$, $\hat{\mathbf{x}}_{0|0} = E[\mathbf{x}_0]$
- Prediction of states: $\hat{\mathbf{x}}_{i|i-1} = \mathbf{F}_{i-1} \hat{\mathbf{x}}_{i-1}$
- Prediction of the state covariance matrix:
$$\Pi_{i|i-1} = \mathbf{F}_{i-1} \Pi_{i-1} \mathbf{F}_{i-1}^T + \mathbf{Q}_{i-1}$$
- Kalman gain matrix:
$$\mathbf{K}_i = \Pi_{i|i-1} \mathbf{H}_{i-1}^T \left(\mathbf{H}_{i-1} \Pi_{i|i-1} \mathbf{H}_{i-1}^T + \mathbf{R}_\mathbf{V} \right)^{-1}$$
- Update of the state estimation:
$$\hat{\mathbf{x}}_i = \hat{\mathbf{x}}_{i|i-1} + \mathbf{K}_i (\mathbf{z}_i - \mathbf{H}_i \hat{\mathbf{x}}_{i|i-1})$$
- Update of the covariance matrix of states:
$$\Pi_i = (\mathbf{I} - \mathbf{K}_i \mathbf{H}_i) \Pi_{i|i-1}$$

Note that the Kalman filtering technique is usually applied to a temporal sequence. Here, it is applied to a spatio-temporal sequence. This spatio-temporal sequence is composed of data from each sensor at each time. Due to its recursive nature, it is more suitable to problems where the measurements are available in a serial manner. Otherwise, if all measurements are available or could be made available (with no serious overhead) at the same time, it is advantageous to applied the Kalman filter in a single joint evaluation (all the spatial sequence at the same time). This is because the Kalman filtering technique is equivalent to the least-squares technique only if the system is linear. For nonlinear problems, the EKF will yield different results depending on the order of processing the measurements one after the other, and may run the risk of being trapped into a local minimum Zhang (1997).

5. SIMULATIONS RESULTS

To demonstrate the efficiency of the proposed approach to enclose the obstacle with an ellipse and to avoid it, a statistical survey was made. We consider a mobile robot with a radius of $R_R = 0.065\ m$ and six infrared range sensors with the maximum detected range equal to $D_L max = 0.30\ m$ (cf. Fig. 5). These sensors are in the front of the robot, with 30° between each pairs of sensor (cf. Fig. 7). The accuracy of the used sensors based on the datasheet is around 10% of $D_L max$. In the simulation, we consider uncertainty range with maximum value of 20% of $D_L max$ ensuring to take the worst range value. The maximum velocity of the robot is 0.4 m/s and the sample time is 0.01 s. For each simulation the robot starts at the same configuration and reach the same final configuration. We do not start to use any method until we have enough range data ($n_{data} \geq 3$).

This survey is used to make a focus around the proposed heuristic method and Kalman filter which gives satisfactory results and this while making an on-line navigation in cluttered environment (cf. Fig. 7).

Fig. 7 shows the trajectory of the robot in the environment with three obstacles. Moreover, the red points represent the range data from the sensor along all the trajectory. The range data buffer used to compute the ellipse parameters is delete to each new obstacle. We observe that the robot avoid the obstacles with a smooth trajectory. This trajectory was obtained while using the on-line obstacle avoidance algorithm Adouane et al. (2011) which takes its parameters (elliptical limit-cycle to follows) from the combination of the proposed heuristic approach and EKF.

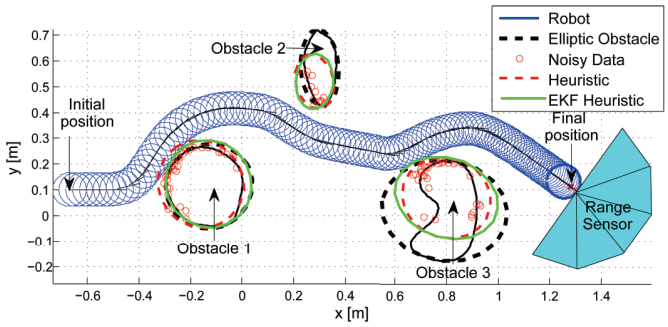

Fig. 7. Robot trajectory using the heuristic and EKF approach to enclosing the obstacle.

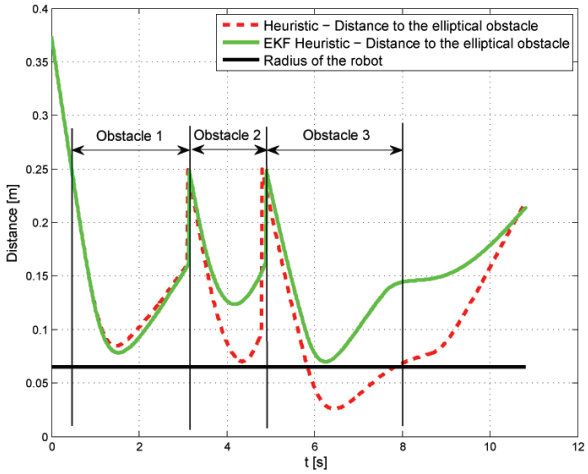

Fig. 8. Distance from the robot to the elliptical obstacles.

Fig. 8 shows the minimum distance between the elliptical obstacles (obtained while knowing all the range data without noise which surround the obstacle) and the position of

the robot along of the elliptical trajectory using only the heuristic method (red dotted line), and the combination of heuristic method and EKF (green line). This figure shows that the robot does never collide with any obstacles when the robust approach is used, therefore, the proposed robust on-line approach is efficient to deal with cluttered and unstructured environment.

Experimentations are implemented using Khepera® III robot (cf. Fig. 9), its kinematic model is given by (2). The navigation is achieved on a platform using the local infrared sensors of the robot. This test demonstrate the efficiency of the proposed robust enclosing ellipse approach. The real trajectory of the robot avoiding two obstacles is given in figure 9. It can be seen that the robot successfully converges to its target after avoiding two obstacles (surrounded with two ellipses of influence).

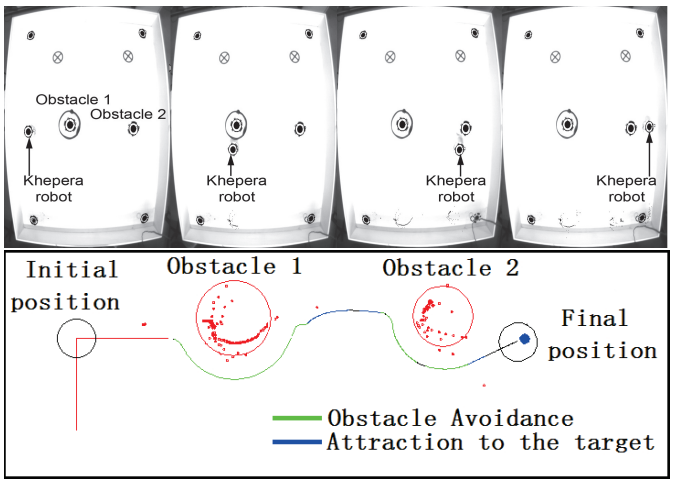

Fig. 9. Top view of the robot trajectory in the platform and observed uncertain range data from the robot.

6. CONCLUSION

This paper proposes robust on-line elliptic trajectory to perform smooth and safe mobile robot navigation. This elliptic limit-cycle trajectory is obtained while using the heuristic method combined with Extended Kalman Filter which deals with the uncertain range data to obtain the parameters of the ellipse which change smoothly. The main contribution of this work is to perform this navigation in a completely reactive way while using only uncertain range data. The obstacle avoidance method permits us to obtain generic and flexible navigation in very cluttered environments. The proposed reactive navigation was embedded in multi-controller architecture and permits for a mobile robot to efficiently navigate in environments with different obstacles shapes. These methods were implemented to evaluate the evolution of obtained ellipse in simulations and experimental form.

In future works, the problem of outliers detection of the range data will be accurately considered and the method will be extended for multi-robot system. Furthermore, the presence of dynamic obstacles will be developed.

REFERENCES

Adouane, L. (2009a). Hybrid and safe control architecture for mobile robot navigation. In *9th Conference on Autonomous Robot Systems and Competitions*. Portugal.

Adouane, L. (2009b). Orbital obstacle avoidance algorithm for reliable and on-line mobile robot navigation. In *9th Conference on Autonomous Robot Systems and Competitions*. Portugal.

Adouane, L., Benzerrouk, A., and Martinet, P. (2011). Mobile robot navigation in cluttered environment using reactive elliptic trajectories. In *18th IFAC World Congress*.

Adouane, L. and Le Fort-Piat, N. (2006). Behavioral and distributed control architecture of control for minimalist mobile robots. *Journal Europen des Systmes Automatiss*, 40(2), pp.177–196.

Benzerrouk, A., Adouane, L., and Martinet, P. (2010). Lyapunov global stability for a reactive mobile robot navigation in presence of obstacles. In *ICRA'10 International Workshop on Robotics and Intelligent Transportation System*.

Brooks, R.A. (1986). A robust layered control system for a mobile robot. *IEEE Journal of Robotics and Automation*, RA-2, pp.14–23.

Burguera, A., Gonzlez, Y., and Oliver, G. (2009). Sonar sensor models and their application to mobile robot localization. *Sensors*, 9(12), 10217 – 10243.

De Maesschalck, R., Jouan-Rimbaud, D., and Massart, D. (2000). The mahalanobis distance. *Chemometrics and Intelligent Laboratory Systems*, 50(1), 1 – 18.

Fouque, C., Bonnifait, P., and Bétaille, D. (2008). Enhancement of global vehicle localization using navigable road maps and dead-reckoning. In *IEEE Position Location and Navigation Symposium*.

Jie, M.S., Baek, J.H., Hong, Y.S., and Lee, K.W. (2006). Real time obstacle avoidance for mobile robot using limit-cycle and vector field method. *Knowledge-Based Intelligent Information and Engineering Systems*.

Khatib, O. (1986). Real-time obstacle avoidance for manipulators and mobile robots. *The International Journal of Robotics Research*, 5, pp.90–99.

Kim, D.H. and Kim, J.H. (2003). A real-time limit-cycle navigation method for fast mobile robots and its application to robot soccer. *Robotics and Autonomous Systems*, 42(1), 17–30.

Levinson, J. and Thrun, S. (2010). Robust vehicle localization in urban environments using probabilistic maps. In *IEEE International Conference on Robotics and Automation*. Alaska, USA.

Rigatos, G.G. (2010). Extended kalman and particle filtering for sensor fusion in motion control of mobile robots. *Mathematics and Computers in Simulation*, 81(3), 590 – 607.

Toibero, J., Carelli, R., and Kuchen, B. (2007). Switching control of mobile robots for autonomous navigation in unknown environments. In *IEEE International Conference on Robotics and Automation*, 1974–1979.

Welzl, E. (1991). Smallest enclosing disks (balls and ellipsoids). In *Results and New Trends in Computer Science*, 359–370. Springer-Verlag.

Xiong, K., Wei, C., and Liu, L. (2011). Robust kalman filtering for discrete-time nonlinear systems with parameter uncertainties. *Aerospace Science and Technology*.

Zhang, Z. (1997). Parameter estimation techniques: A tutorial with application to conic fitting. *Image and Vision Computing*, 15, 59 – 76.